International Journal of Heat and Fluid Flow 30 (2009) 796–803

Contents lists available at ScienceDirect

International Journal of Heat and Fluid Flow

journal homepage: www.elsevier.com/locate/ijhff

Film flow around a fast rotating roller

Seung-Hwan Yu, Kwan-Soo Lee *, Se-Jin Yook

School of Mechanical Engineering, Hanyang University, 17 Haengdang-dong, Seongdong-gu, Seoul 133-791, Republic of Korea

ARTICLE INFO

Article history:
Received 23 July 2008
Received in revised form 29 December 2008
Accepted 22 January 2009
Available online 27 February 2009

Keywords:
Film flow
Rotating roller
VOF method

ABSTRACT

In this study, the film thickness around the roller is numerically estimated using the volume of fluid (VOF) method to clarify the film-formation process around the rotating roller. Parametric studies were performed to compare the effects of ink properties (viscosity, surface tension) and operational conditions (roller rotation speed, initial immersed angle) on film thickness. The viscosity of the ink and the speed of rotation of the roller were found to be the dominant factors that determine the ink film thickness. In addition, a correlation equation is proposed to predict the thickness of the ink film around a printing roller rotating at a speed of 20–30 rad/s, as a function of angular position, angular velocity, and viscosity.

1. Introduction

Recently, the liquid coating is widely used in many industrial applications. For example, gravure printing is adopted to coat paper, fabric or metal sheets with decorative or protective materials. A schematic of gravure printing is depicted in Fig. 1. The printing process is as follows. Ink is supplied into the engraved cell, and the doctor blade removes the excess ink. Subsequently, the force acting on the cell transfers the ink onto the substrate, which is fed between the impression roller and printing roller. To achieve a high-quality print with accurate dimensions, the amount of ink supplied to the cell must be precisely controlled. When the excess ink is doctored, an important factor is the ink film thickness around the rotating printing roller. If the ink film is too thick, the excess ink outside the engraved cell will not be perfectly doctored, resulting in poor quality printing. However, to remove it completely, excessive doctoring will reduce the useful life of the printing machine due to wear of the doctor blade and the printing roller surface. If the ink film is too thin, obtaining uniform prints becomes difficult. Therefore, controlling the ink film thickness before doctoring the excess ink is extremely important in ensuring both uniform print quality and the durability of the printing machine.

Numerous studies have analyzed the liquid film thickness around a rotating roller for a Newtonian fluid. Spiers et al. (1974) divided the film on a vertically moving plate partially immersed in a liquid into three regions, the static meniscus, dynamic meniscus, and constant-film-thickness regions, and proposed theoretical models to predict film thickness. Tharmalingam and Wilkinson (1978) suggested models to predict film thickness around a rotating roller based on the model of Spiers et al. (1974) by considering the effects of the immersion and inspection angles and compared predictions with experimental data. Campanella and Cerro (1984) showed the effects of immersion angle, roller radius and speed of rotation on film thickness using the rapid-flow approximation derived by Cerro and Scriven (1980).

These studies dealt with the film flow around a rotating roller with an angular speed lower than 10 rad/s. When the linear speed of the roller surface is above 50 cm/s, measuring film thickness experimentally becomes difficult due to instability of the flow (Campanella and Cerro, 1984). A theoretical prediction of film thickness is also hard due to the disappearance of the static meniscus region. Furthermore, as the viscosity of ink changes with dilution by the solvent, the effect on film thickness of a change in viscosity must be considered.

In this study, the film flow around a rotating roller partially immersed in ink was numerically analyzed at relatively high speeds of rotation. The parameters that affect film thickness were first categorized into two groups. The "property parameters" were the viscosity and surface tension, which were dependent on the solvent dilution of the ink. The "operation parameters" were the angular velocity and the initial immersion angle of the printing roller. Parametric studies were then performed to compare the effects of these four parameters on film thickness. Based on the results, we propose a correlation equation that can predict film thickness on a roller rotating at high speed.

2. Numerical model

Fig. 2 shows a schematic of the computational domain for this study. The pan was 0.6 m wide and 0.6 m high while the diameter of the roller was 0.15 m. The initial thickness of the ink was

* Corresponding author. Tel.: +82 2 2220 0426; fax: +82 2 2295 9021.
E-mail address: ksleehy@hanyang.ac.kr (K.-S. Lee).

0142-727X/$ - see front matter Crown Copyright © 2009 Published by Elsevier Inc. All rights reserved.
doi:10.1016/j.ijheatfluidflow.2009.01.013

Nomenclature

Ca	capillary number $\left(\frac{\mu U}{\sigma}\right)$
F	force (N)
G	gravitational force (N/m^2·s)
h	film thickness (cm)
N	normal vector
P	pressure (N/m^2)
R	radius of a roller (m)
T	film thickness number $(h(\rho g \sin\theta_i/\mu U)^{1/2})$
U	roller surface velocity ($r\omega$)
V	velocity (m/s)
v	tangential vector
We	Webber number $\left(\frac{\rho L U^2}{\sigma}\right)$
x	film position (cm)

Greek symbols

α	volume fraction
κ	curvature (m^{-1})
μ	viscosity (N/m^2·s)
θ	angular position (°)
ρ	density (kg/m^3)
σ	surface tension coefficient (N/m)
ω	angular velocity (rad/s)

Subscripts

i	Immersion
k	kth phase
r	Reference
SF	surface tension source term
w	wall adhesion

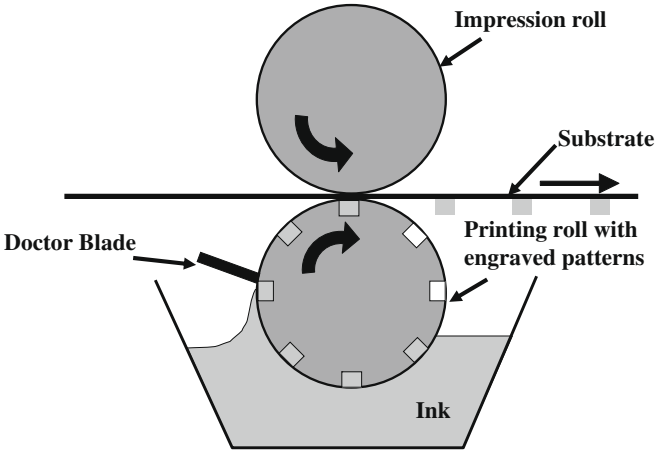

Fig. 1. Schematic of gravure printing.

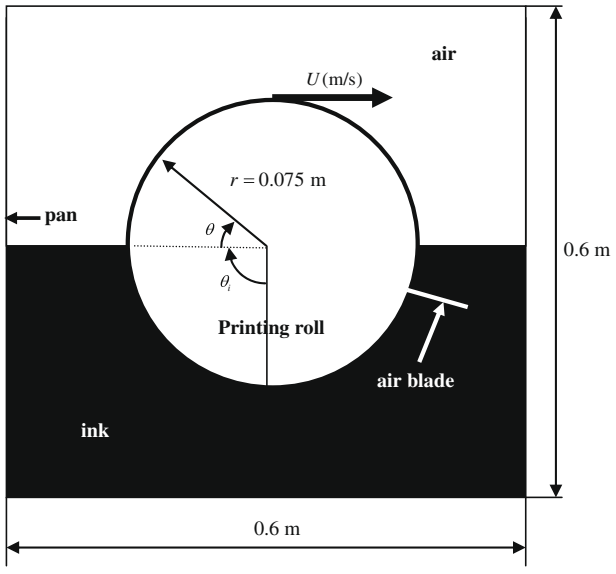

Fig. 2. The computational domain used for gravure printing.

assumed to be half of the pan height as shown in Fig. 2. This corresponds to 90° for the immersion angle (θ_i). The doctor blade used in the actual gravure printing apparatus was not considered in the numerical calculation because it forcibly reduces the film thickness and the characteristics of film flow cannot be observed. For the numerical analysis, the following assumptions were made.

(1) The flow is unsteady, laminar, incompressible and two-dimensional.
(2) The properties of the fluids are independent of temperature.
(3) The two fluids (air and ink) are immiscible, and therefore a free surface exists.
(4) The contact angle between the ink and the roller is 90°. (The contact angle is usually smaller than 90°. However, the effect of contact angle is negligible because the film flow entirely covers the roller surface. Therefore, the contact angle of 90° is assumed for the VOF modeling.)
(5) Air entrainment into the ink at the right-hand side of the roller, caused by the rotation, was prevented by the air-blade. Without an air-blade, air entrainment into the ink at the right-hand side of the roller, caused by the high speed rotation, will happen. Then, air bubbles can move along the roller surface and make the film flows unstable (Bolton and Middleman, 1980). In order to forcibly remove the air entrainment, the air-blade was installed at the right side of roller as shown in Fig. 2.

2.1. Governing equations

The volume of fluid (VOF) method (Hirt and Nichols, 1981) was adopted in the present study. The VOF method was used by many researchers to simulate the flow of two immiscible fluids (Cook and Behnia, 2001; Nikolopoulos et al., 2005; Lan et al., 2008). To calculate the interface between the two fluid phases, the piecewise linear interface calculations (PLIC) method (Rider and Kothe, 1998) was used. It assumes that the interface between two fluids has a linear slope in each cell, and uses this linear shape to calculate the advection of fluid through the cell faces. The first step in this reconstruction scheme is to calculate the position of the linear interface relative to the center of each partially-filled cell, based on the information about volume fraction and its derivatives in the cell. The second step is to calculate the advecting amount of fluid through each face using the computed linear interface representation and information about the normal and tangential velocity distribution on the face. The third step is to calculate the volume fraction in each cell using the balance of fluxes calculated during the previous step.

In each phase, the mass conservation equation is given by

$$\frac{\partial(\rho)}{\partial t} + \nabla \cdot (\rho \vec{v}) = 0 \tag{1}$$

and the momentum conservation equation is

$$\frac{\partial}{\partial t}(\rho \vec{v}) + \nabla \cdot (\rho \vec{v}\,\vec{v}) = -\nabla P + \mu \nabla^2 \vec{v} + \rho \vec{g} + \vec{F}_{SF}, \tag{2}$$

where F_{SF} is the continuum surface force vector. The density of the mixture is calculated as

$$\rho = \alpha_1 \rho_1 + \alpha_2 \rho_2, \tag{3}$$

where α_k ($0 \leqslant \alpha_k \leqslant 1$) is the volume fraction of the kth fluid, $k = 1$ represents air, and $k = 2$ represents ink. When α_k is 0, the kth fluid does not exist in the computational domain, and when α_k is 1, only the kth fluid exists in the computational domain. The fluid viscosity, μ, was calculated as

$$\mu = \frac{\alpha_1 \rho_1 \mu_1 + \alpha_2 \rho_2 \mu_2}{\alpha_1 \rho_1 + \alpha_2 \rho_2}. \tag{4}$$

The correlation between the air (α_1) and ink (α_2), was obtained from the following equations:

$$\frac{\partial \alpha_2}{\partial t} + \vec{v} \cdot \nabla \alpha_2 \quad \text{and} \tag{5}$$

$$\alpha_1 + \alpha_2 = 1. \tag{6}$$

The surface tension force was calculated with the continuum surface force model (Brackbill et al., 1992):

$$F_{SF} = \sigma \kappa n \left[\frac{\alpha_1 \rho_1 + \alpha_2 \rho_2}{1/2(\rho_1 + \rho_2)}\right], \tag{7}$$

$$n = \nabla \alpha_2, \text{ and} \tag{8}$$

$$\kappa = -(\nabla \cdot \hat{n}) = \frac{1}{|n|}\left[\left(\frac{n}{|n|} \cdot \nabla\right)|n| - (\nabla \cdot n)\right], \tag{9}$$

where **n** is the surface normal vector, $\hat{n}$ is the unit normal vector, and κ is the curvature. F_{SF} represents the source term in the momentum equation. The wall adhesion modifies the surface normal vector as

$$\hat{n} = \hat{n}_w \cos\theta_w + \hat{v}_w \sin\theta_w, \tag{10}$$

where θ_w, $\hat{n}_w$ and $\hat{v}_w$ are the contact angle at wall and the unit vectors normal and tangent to the wall, respectively.

2.2. Boundary and initial conditions

The boundary conditions are prescribed as follows.

(1) At the contact region around the rotating roller,

$$V_{\text{roller,outer}} = V_{\text{fluid,contact}} = r\omega. \tag{11}$$

(2) At the contact region between the fluids and the wall,

Table 1
Properties of each phase.

Phase	ρ (kg/m^3)	μ (N/m^{2}s)	σ (N/m)
Air	1.225	1.789×10^{-5}	–
Ink	1560	0.136	0.035

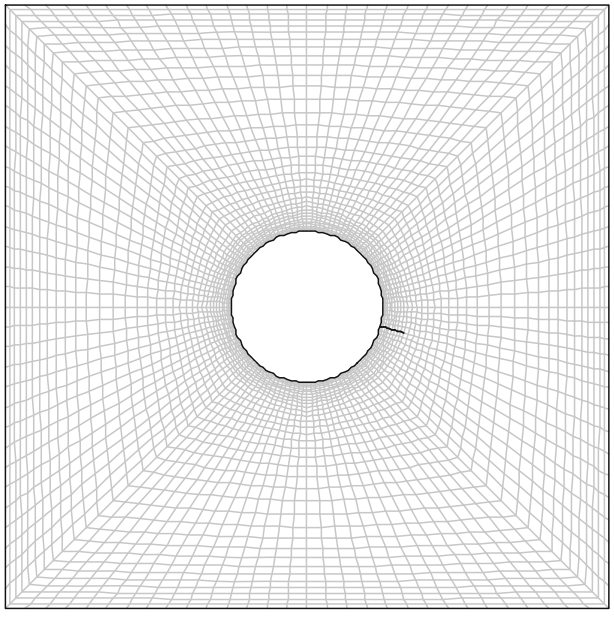

Fig. 3. Schematic of the utilized grid distribution.

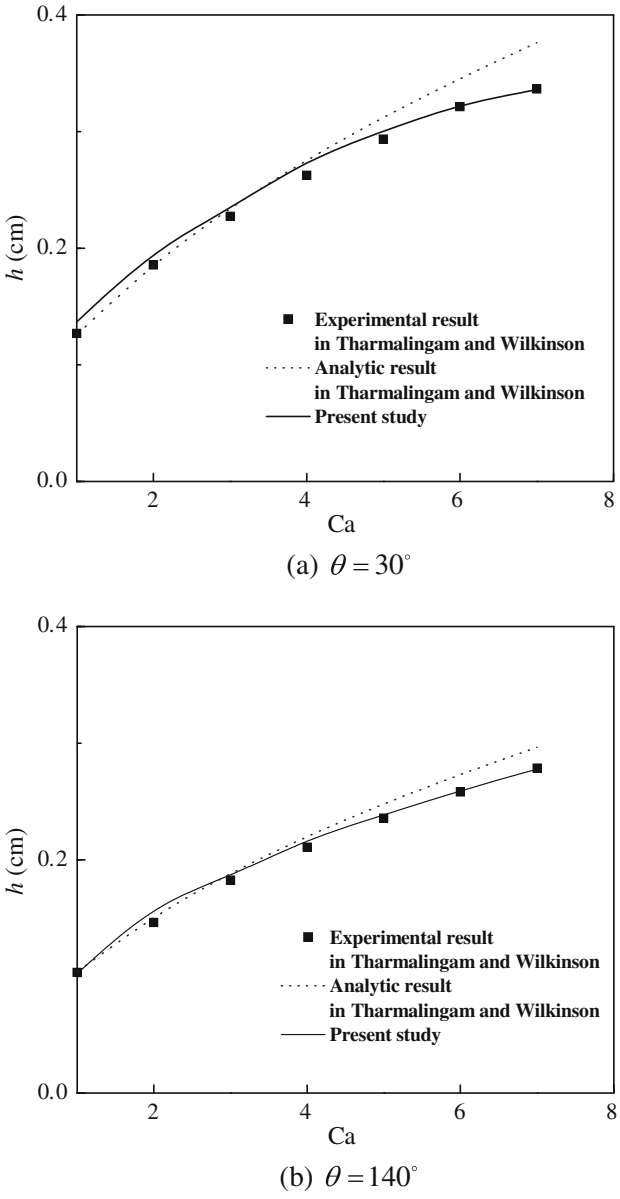

Fig. 4. Comparison of film thicknesses with the results in in Tharmalingam and Wilkinson (1978).

$$V_{\text{ink,wall}} = 0. \quad (12)$$

The initial conditions for the volume fractions are

$$\alpha_1 = 1 \text{ for the cell filled with air}, \quad (13)$$

$$\alpha_2 = 1 \text{ for the cell filled with ink, and} \quad (14)$$

$$\alpha_1 = \alpha_2 = 0.5 \text{ for the cell representing the interface between the air and the ink.} \quad (15)$$

2.3. Force calculation

The viscous force, inertia, gravitational force, and surface tension force acting on the film flow around the rotating roller were calculated as (Rebouillat et al., 2002)

$$F_{\text{viscosity}} = \left(\mu \frac{r\omega}{h}\right) h^2, \quad (16)$$

$$F_{\text{inertia}} = \left(\rho (r\omega)^2\right) h^2, \quad (17)$$

$$F_{\text{surface tension}} = \sigma h, \text{ and} \quad (18)$$

$$F_{\text{gravity}} = -(\rho g \cos\theta) h^3. \quad (19)$$

2.4. Numerical method

Numerical simulation was conducted using Fluent V6.2, a commercially available CFD code based on a finite volume method. The fractional step algorithm was employed to couple velocity and pressure. Mass and momentum equations were solved using a second-order upwind scheme for space, while a first-order implicit method was used for the time discretization. Pressure interpolation was performed using a body-force-weighted scheme that performs better for VOF simulations of fluids having a substantial density difference. Grid-independence tests were performed by varying grid number (2520–28,800) and time step (0.01 s–0.00001 s) to determine an optimum test condition. The grid number and time step were chosen to be 45×120 and 10^{-4} s, respectively, such that the change in film thickness was within 0.5%. Fig. 3 shows a schematic of the utilized grid distribution. The convergence criterion was 10^{-5} for both the continuity and momentum equations at each time step. The properties used for both air and ink are listed in Table 1.

3. Results and discussion

The numerical model proposed in the previous section was validated by applying the conditions in Tharmalingam and Wilkinson (1978) and comparing numerical results with their experimental data. Fig. 4 shows a comparison of the film thickness at $\theta = 30°$ and 140°, when $\rho = 902.0$ kg/m^3, $\mu = 0.691$ kg/m s^2, $\sigma = 0.035$ N/m, and $\theta_i = 90°$. The x-axis is the capillary number, Ca($=\mu U/\sigma$) and the y-axis is the film thickness. The previous theoretical prediction of Tharmalingam and Wilkinson (1978) deviated from their experimental data at higher Ca, which means higher rotating speed, because the static meniscus region used for the initial conditions in Tharmalingam and Wilkinson (1978) disappeared and the inertial force became relatively larger. However, our numerical results show better agreement with the experimental data than the theoretical prediction, which implies that the numerical model of the present study can be extended to analysis of film flows around rollers rotating at relatively high speeds.

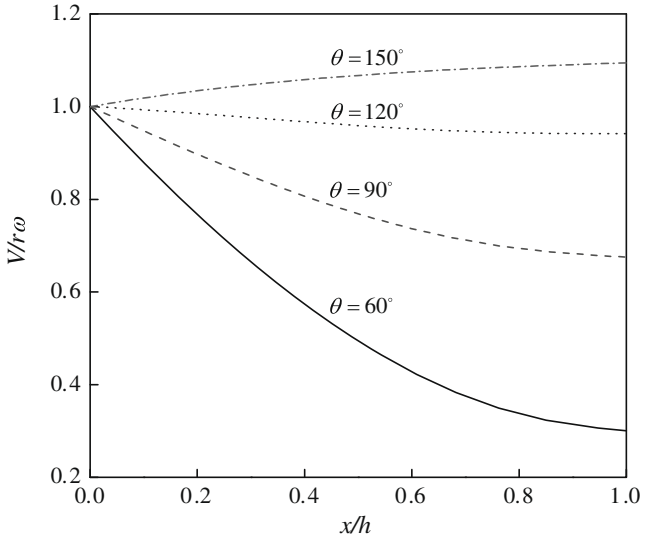

Fig. 6. Film velocity as a function of non-dimensional radial position ($\omega = 20$ rad/s, $\theta_i = 90°$).

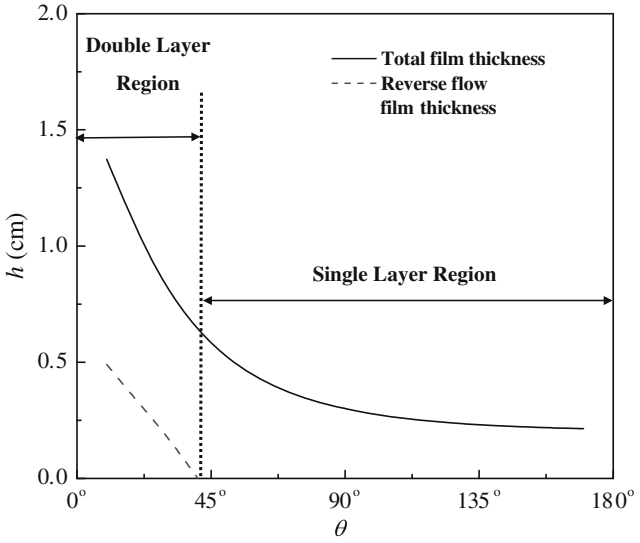

Fig. 5. Profiles of film thicknesses ($\omega = 20$ rad/s, $\theta_i = 90°$).

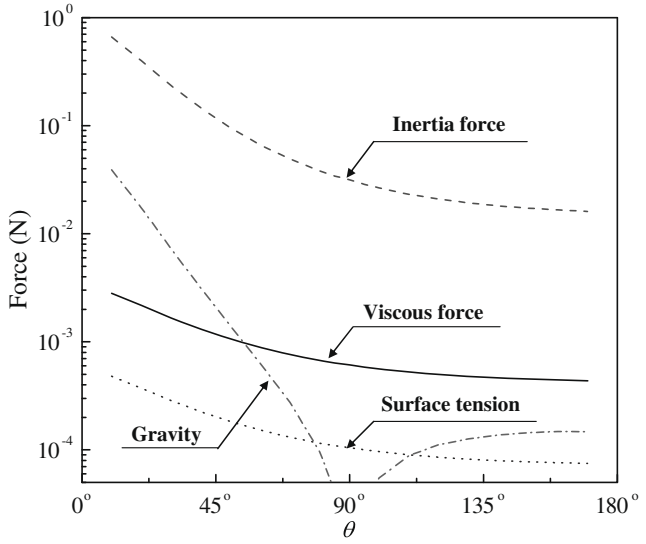

Fig. 7. Profiles of relative forces. Note that the absolute values were considered for comparison. ($\omega = 20$ rad/s, $\theta_i = 90°$).

3.1. Film thickness according to angular position

Fig. 5 shows the film thickness as a function of angular position when the film flow was fully developed, keeping $\omega = 20$ rad/s and $\theta_i = 90°$. The film flow was divided into a double-layer region ($0° < \theta < 39°$) and a single-layer region ($39° < \theta < 180°$). Within the double-layer region, two flows occurred, i.e. forward and reverse flow relative to the direction of roller rotation (see Fig. 8c). In the single-layer region, only forward flow existed. The thickness of the reverse flow was greatest at $\theta = 0°$, when the effect of gravity was greatest. The tangential magnitude of the effect of gravity decreased with increasing value of the angular position, θ, until $\theta > 39°$, when no reverse flow was seen.

Fig. 6 shows the velocity distribution according to the angular position, θ, to investigate changes in film thickness in the single-layer region. The x-axis is the height within the film in the normal direction to the roller surface normalized by the film thickness, and the y-axis is the ratio of the film velocity to the speed of the rotating roller. When $\theta < 90°$, the tangential magnitude of gravity, which acted in the opposite direction to roller rotation, became smaller as θ increased, and thus the film velocity increased. When $\theta > 90°$, the tangential magnitude of gravity accelerated the film flow. As a result, for $\theta > 120°$, the film velocity was larger than the velocity of the rotating roller surface, and the film flow became almost fully developed. Accordingly, the resultant film thickness decreased exponentially and reached a constant value as the angular position increased, as shown in Fig. 5.

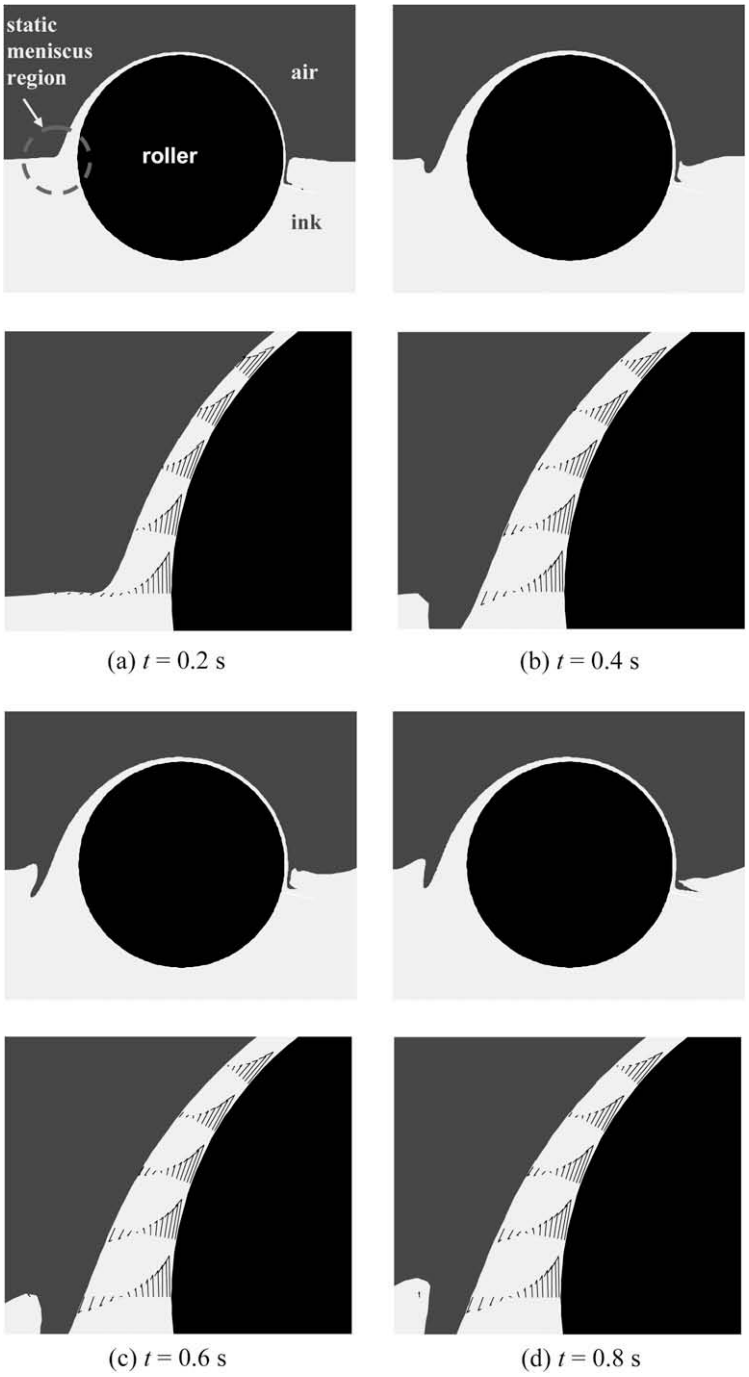

Fig. 8. Variation in the contours of phases around the rotating roller with time ($\omega = 20$ rad/s, $\theta_i = 90°$).

3.2. Analysis of different forces on film flow

Fig. 7 shows the various forces calculated with Eqs. (16)–(19) acting on the film flow according to the angular position under the conditions of $\omega = 20$ rad/s and $\theta_i = 90°$. The absolute values of the forces were compared; as the roller was rotating at a relatively high speed, the inertial force was the highest in all regions, followed by the force of gravity in the double-layer region or the viscous force in the single-layer region. The surface tension force was negligible in all regions. From these results, the angular velocity of the roller, initial immersion angle, and ink viscosity clearly affect film thickness. For $\theta > 100°$, the changes in the magnitude of forces were small because the film flow became almost fully developed and film thickness approached a constant value.

3.3. Film formation process and air-blade position

Fig. 8 shows the contour of phases and velocity vectors around the rotating roller under the conditions of $\omega = 20$ rad/s and $\theta_i = 90°$. Both the range of the double-layer region and film thickness increased with elapsing time. At $t = 0.2$ s, the static meniscus region, where the surface tension is dominant, appeared and the reverse flow was very weak in comparison. Subsequently, the reverse flow increased greatly due to the effect of gravity, and the static meniscus region disappeared. At $t = 0.8$ s, the film flow was almost fully developed, approaching the quasi-steady state.

Fig. 9 indicates the effect of air-blade position ($195° \leqslant \theta \leqslant 270°$) on the film thickness. As the angular position of air-blade increased, the film thickness slightly decreased because the time during which the ink flow was influenced by the rotating roller was shortened after the interruption by the air-blade. Therefore, we selected the air-blade position of $\theta = 195°$ to minimize decrease of film thickness by the air-blade.

3.4. Effects of ink properties and operational conditions on film thickness

Parametric studies were carried out to compare the effects of ink viscosity, surface tension, angular velocity, and initial immersion angle on film thickness. The reference values of these parameters were 0.136 N/m^2 s, 0.035 σ/m, 20 rad/s, and 90°, respectively. As shown in Fig. 10, film thickness increased with increasing ink viscosity because the momentum transfer of the film flow from the surface of the rotating roller increases at higher viscosity. In addition, the rate of change of the film thickness in the double-layer region was larger due to the force of gravity. In Fig. 11, the effect of surface tension is shown to be negligible, due to the absence of a meniscus region at $\theta = 0°$. Furthermore, the capillary number, the ratio of the viscous force to the surface tension force, ranged from 2.3 to 11.6, and the Webber number, the ratio of inertial force to surface tension force, varied from 2817 to 16,900. Accordingly, it is clear that the effect of surface tension force was much smaller than the viscous or inertial forces.

Fig. 12 shows the effect of angular velocity on film thickness. As the angular velocity of the roller increased, both film thickness and the width of the double-layer region increased because an increase in the angular velocity resulted in an increase in the inertial force that was dominant in all regions. The effect of the immersion angle on film thickness is illustrated in Fig. 13. A larger initial immersion angle (θ_i) reduces the duration for gravity to act as a flow resistance in the double-layer region, thus decreasing the amount of flow

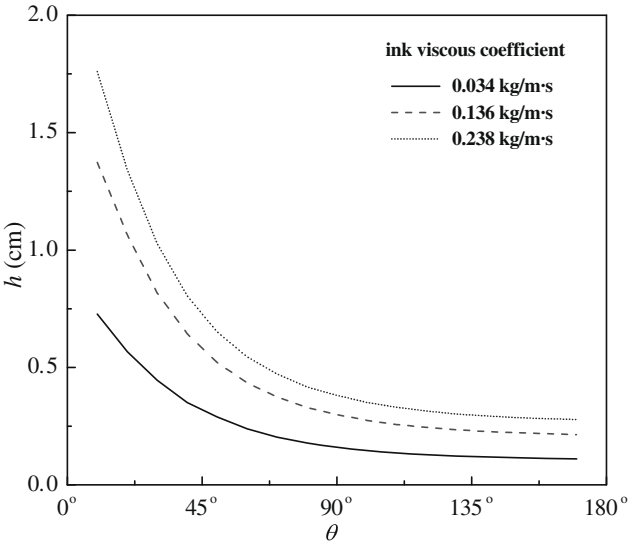

Fig. 10. The effect of ink viscosity on film thickness.

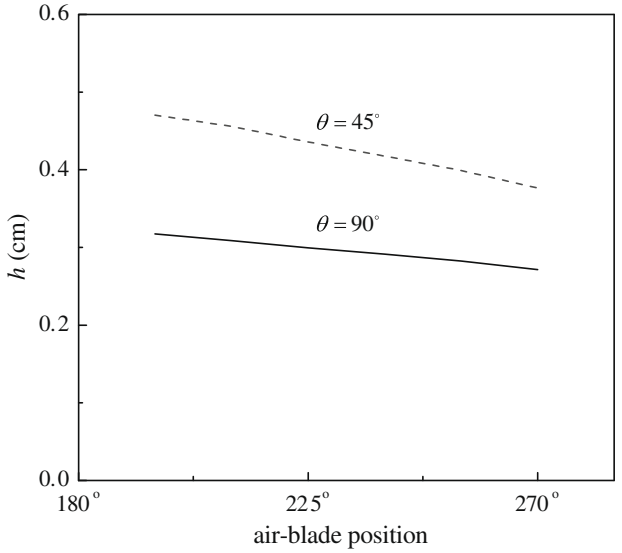

Fig. 9. The effect of air-blade position on film thickness.

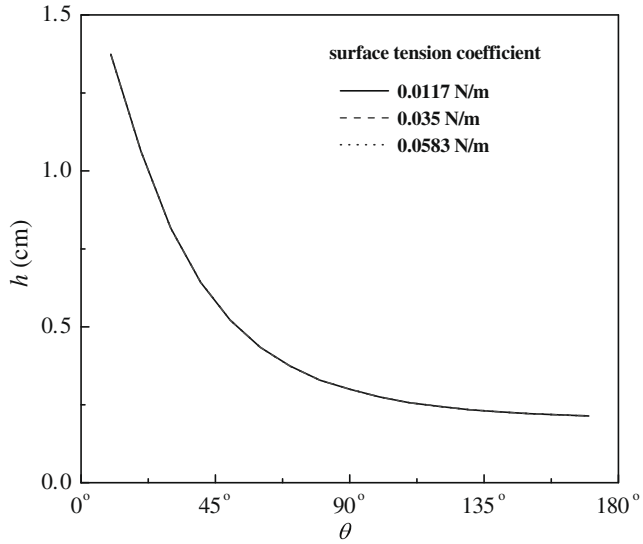

Fig. 11. The effect of surface tension on film thickness.

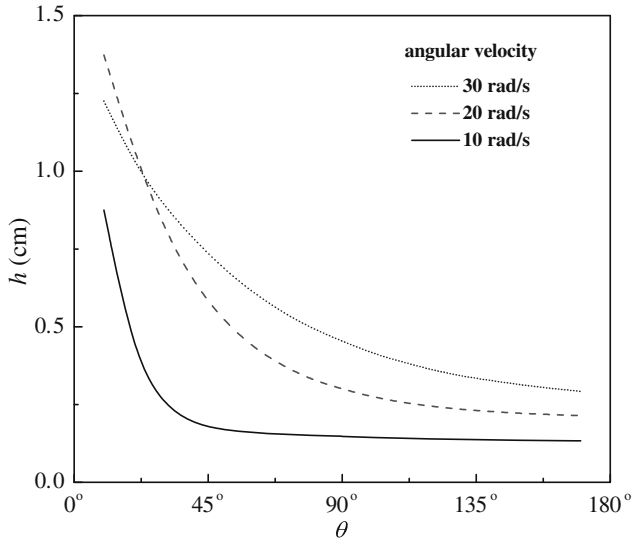

Fig. 12. The effect of speed of rotation on film thickness.

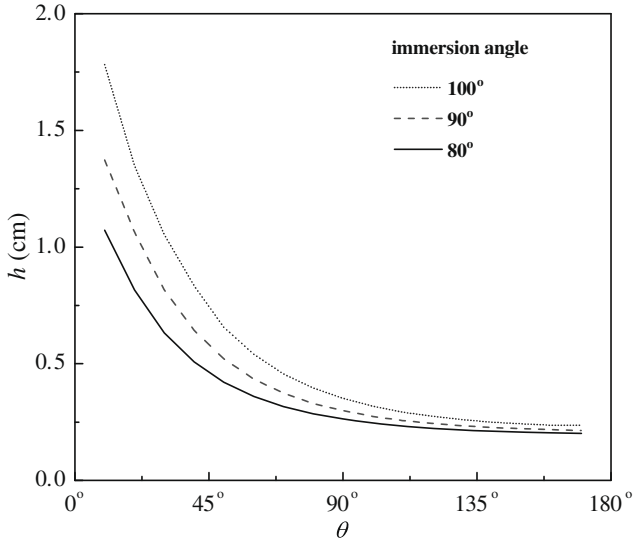

Fig. 13. The effect of initial immersion angle on film thickness.

back to the ink pool. This results in an increase in film thickness. However, because the magnitude of the effect of gravity on film flow increases in proportion to increased film thickness for a larger immersion angle, the rate of decrease of film thickness in the double-layer region is greater and the double-layer region itself widens. In the single-layer region, a negligible increase in film thickness was seen with an increase in immersion angle.

3.5. Prediction of film thickness

The previous section analyzed the effects of various parameters on film thickness. The surface tension and initial immersion angle showed little effect on film thickness in the single-layer region, as shown in Figs. 11 and 13, while the viscosity of the ink and the angular velocity of the roller had a great effect on film thickness, as shown in Figs. 10 and 12. Thus, the viscosity of the ink and the angular velocity of the roller are considered primary parameters that dominantly affect film thickness. For the initial immersion angle of 90°, a correlation equation to predict film thickness number is proposed as follows, when the ranges of viscosity and angular velocity considered for this correlation were 0.068 kg/m s $\leqslant \mu \leqslant$ 0.238 kg/m s and 10 rad/s $\leqslant \omega \leqslant$ 30 rad/s, respectively.

$$T = a + b/(\theta/\theta_r) + c(\mu/\mu_r) \tag{20}$$

where, $a = -2.8305(\omega/\omega_r)^4 + 11.5177(\omega/\omega_r)^3 - 16.0412(\omega/\omega_r)^2 + 8.6494(\omega/\omega_r) - 1.1076$, $b = 4.2848(\omega/\omega_r)^4 - 18.4430(\omega/\omega_r)^3 + 27.4049(\omega/\omega_r)^2 - 15.6484(\omega/\omega_r) + 3.1124$, $c = -0.6878(\omega/\omega_r)^4 + 2.9330(\omega/\omega_r)^3 - 4.3577(\omega/\omega_r)^2 + 2.5674(\omega/\omega_r) - 0.5188$, $\mu_r = 0.136$ kg/m s, $\omega_r = 20$ rad/s, and $\theta_r = 90°$.

When the speed of rotation of the roller is relatively low, i.e. $\omega < 10$ rad/s, film thickness can be predicted by the theory of Tharmalingam and Wilkinson (1978). At higher rotation speeds, i.e. 10 rad/s $< \omega <$ 30 rad/s, Eq. (20) can be used to predict film thickness, since their analytical model deviates from the experimental data with increasing speed of rotation as shown in Fig. 4. Note that μ and ω are important parameters to control film thickness as analyzed in the previous section. Once the film thickness number (T) is predicted using Eq. (20), the film thickness (h) at relatively high rotation speed can be obtained from the definition of film thickness number used by Tharmalingam and Wilkinson (1978), i.e. $T = h(\rho g \sin\theta_i/\mu U)^{1/2}$.

4. Conclusions

A numerical model was developed to analyze the film flow around a rotating roller partially immersed in ink and rotating at high speed. The results from this model showed good agreement with the experimental data of Tharmalingam and Wilkinson (1978). Parametric studies were performed with the model to compare the effects of ink viscosity, surface tension, angular velocity, and immersion angle on film thickness. From the results obtained, a correlation to predict film thickness on a roller rotating at high speed was proposed. The key results of this study are summarized as follows.

As the angular position increased, the total film thickness decreased exponentially before reaching a constant value. The film flow showed two distinct regions. In the double-layer region, both forward and reverse flows occurred. In the single-layer region, only forward flow was present. The magnitudes of different forces in the film flow were compared. In order of decreasing magnitude, the forces present in the double-layer region were the inertial, gravitational, viscous, and surface tension forces, while in the single-layer region the forces present were the inertial, viscous, gravitational, and surface tension forces. The film thickness increased with an increase in ink viscosity, angular velocity, and initial immersion angle. The viscosity of the ink and the speed of rotation of the roller were the dominant parameters to control film thickness in all film regions. The film thickness on the roller rotating at relatively high speed (i.e. 10 rad/s $\leqslant \omega \leqslant$ 30 rad/s) can be predicted by Eq. (20).

Acknowledgement

This research was supported by the Seoul R&BD program.

References

Bolton, B., Middleman, S., 1980. Air entrainment in a roll coating system. Chem. Eng. Sci. 35, 597–602.
Brackbill, J.U., Kothe, D.B., Zemach, C., 1992. A continuum method for modeling surface tension. J. Comput. Phys. 100, 335–354.
Campanella, O.H., Cerro, R.L., 1984. Viscous flow on the outside of a horizontal rotating cylinder: the roll coating regime with a single fluid. Chem. Eng. Sci. 39, 1443–1449.
Cerro, R.L., Scriven, L.E., 1980. Rapid free surface film flows. An integral Approach. Ind. Eng. Chem. Fundam. 19, 40–50.

Cook, M., Behnia, H., 2001. Bubble motion during inclined intermittent flow. Int. J. Heat Fluid Flow 22, 543–551.
Hirt, C.W., Nichols, B.D., 1981. Volume of fluid (VOF) method for the dynamics of free boundaries. J. Comput. Phys. 39, 201–225.
Lan, H., Friedrich, M., Armaly, B.F., Drallmeier, J.A., 2008. Simulation and measurement of 3D shear-driven thin liquid film flow in a duct. Int. J. Heat Fluid Flow 29, 449–459.
Nikolopoulos, N., Theodorakakos, A., Bergeles, G., 2005. Normal impingement of a droplet onto a wall film: a numerical investigation. Int. J. Heat Fluid Flow 26, 119–132.
Rebouillat, S., Steffenino, B., Salvador, B., 2002. Hydrodynamics of high-speed fibre impregnation: the fluid layer formation from the meniscus region. Chem. Eng. Sci. 57, 2953–3966.
Rider, W.J., Kothe, D.B., 1998. Reconstructing volume tracking. J. Comput. Phys. 141, 112–152.
Spiers, R.P., Subbaraman, C.V., Wilkinson, W.L., 1974. Free coating of a Newtonian liquid onto a vertical surface. Chem. Eng. Sci. 29, 389–396.
Tharmalingam, S., Wilkinson, W.L., 1978. The coating of Newtonian liquids onto a rotating roll. Chem. Eng. Sci. 33, 1481–1487.